NANO LETTERS

Letter

pubs.acs.org/NanoLett

Infrared Spectroscopy of Tunable Dirac Terahertz Magneto-Plasmons in Graphene

Hugen Yan,[†,§,*] Zhiqiang Li,[‡,§] Xuesong Li,[†] Wenjuan Zhu,[†] Phaedon Avouris,[†,*] and Fengnian Xia*[,†]

[†]IBM T. J. Watson Research Center, Yorktown Heights, New York 10598, United States

[‡]National High Magnetic Field Laboratory, Tallahassee, Florida 32310, United States

Supporting Information

ABSTRACT: We present infrared spectroscopy study of plasmon excitations in graphene in high magnetic fields. The plasmon resonance in patterned graphene disks splits into edge and bulk plasmon modes in magnetic fields. Remarkably, the edge plasmons develop increasingly longer lifetimes in high fields due to the suppression of backscattering. Moreover, due to the linear band structure of graphene, the splitting of the edge and bulk plasmon modes develops a strong doping dependence, which differs from the behavior of conventional semiconductor two-dimensional electron gas (2DEG) systems. We also observe the appearance of a higher order mode indicating an anharmonic confinement potential even in these well-defined circular disks. Our work not only opens an avenue for the investigation of the properties of Dirac magnetoplasmons but also supports the great potential of graphene for tunable terahertz magneto-optical devices.

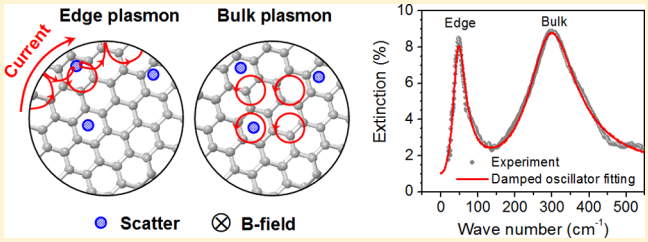

KEYWORDS: *Graphene, magnetoplasmon, edge-magnetoplasmon, terahertz*

Plasmons, collective oscillations of charged carriers, offer opportunities to combine electronics and photonics at the nanoscale, which will enable a broad range of applications.[1] Graphene is emerging as a very promising plasmonic material[2−7] due to its carrier density tunability and high carrier mobility. Recent optical experiments have revealed the great prospects of plasmons in graphene for photonic device applications in the infrared (IR) and terahertz frequency ranges.[5−7] Theoretical studies have predicted many new phenomena and applications in photonics, transformation optics, and quantum optics due to the unique properties of Dirac plasmons.[2−4] Moreover, plasmons are important for understanding the many-body physics of graphene.[8,9] Unlike plasmons in metals,[1] the plasmons in graphene are expected to be strongly affected by an external magnetic field due to a comparable cyclotron frequency[10−12] and plasmon frequency. Therefore, it is of great fundamental and practical interest to explore the response of plasmons in graphene to a magnetic field.

Here, we report an IR study of magnetoplasmons in micrometer size disk arrays of graphene. The plasmon resonance in these structures splits into two modes in magnetic fields with different field dispersions, which can be assigned to an edge mode and a bulk mode.[13] Most interestingly, we find that the plasmon lifetime can be dramatically modified by a magnetic field. The edge mode develops a much longer lifetime than that at zero field, not previously observed in the high-frequency plasmons (terahertz) of the extensively studied, conventional two-dimensional electron (2DEG) systems.[13−15] This behavior may appear to be counterintuitive since imperfections of the edges may be expected to introduce more scattering and decrease the plasmon lifetime. We show that this behavior is attributed to increasing quasi-one-dimensional field-induced confinement of the carriers and the resulting suppression of their backscattering.[16] Moreover, the splitting of the edge and bulk modes has a strong doping dependence due to the tunable cyclotron mass,[17,18] differing from that in conventional 2DEG with parabolic electronic band structure. Finally, the appearance of a higher order plasmon mode provides insights into the confinement potential of the disks.[19] The plasmons tunable by magnetic field, doping, nanostructure dimensions and graphene layer numbers demonstrated here and elsewhere[5−7] affirm the great potential of graphene for tunable terahertz magneto-optical devices, and open an avenue for studying the intriguing physics of graphene edges and of plasmons at both the classical and quantum Hall regimes.[10,20−22]

Single layer graphene grown on copper foil through chemical vapor deposition is used.[23] The graphene on copper is first transferred to a highly resistive silicon substrate with a 90 nm thermal oxide layer. The graphene disk arrays are then fabricated using standard e-beam lithography and plasma etching. The disks are arranged in a triangular lattice, and the total area for a typical array is 3.6 mm × 3.6 mm. The as-prepared graphene samples are hole-doped with Fermi energy of around 0.3 eV. By exposing the sample to the nitric acid

Received: April 30, 2012
Revised: June 1, 2012
Published: June 12, 2012

   dx.doi.org/10.1021/nl3016335 | *Nano Lett.* 2012, 12, 3766−3771

vapor, the doping level can be enhanced dramatically.[7,24] On the other hand, baking the samples at 170 °C in air usually leads to reduction in doping concentration. During the measurement, the samples and reference silicon substrates are mounted in a sample holder, which is inserted into a liquid helium cryostat and cooled via helium exchange gas to a temperature of 4.5 K. Unpolarized infrared light from a Bruker IFS-113 Fourier transform spectrometer is delivered to the sample via a light pipe, and the transmitted light is detected by a composite Si bolometer. The measurements are performed in a superconducting magnet in the Faraday geometry (magnetic field perpendicular to the sample surface). The transmission through the graphene disk array T and through the reference substrate T_s are measured in a magnetic field from 0 to 17.5 T.

Figure 1a shows a scanning electron micrograph of a sample with a 3 μm diameter (d = 3 μm) disk array arranged in a triangular lattice, where the lattice constant is 4.5 μm. Figure 1b shows the extinction spectrum ($1 - T/T_s$) of such an array (Fermi level E_f = −0.54 eV, determined from the cyclotron mass, see Supporting Information) at zero magnetic field. The spectrum is referenced to the transmission T_s through a bare substrate without graphene.[24] The dominant feature in this spectrum is a dipolar plasmonic resonance at ~130 cm^{-1}. As in the case of conventional 2DEG,[14] this mode can be well described as a damped oscillator in the quasi-static limit as shown by the fitting curve (see Supporting Information).[4,14]

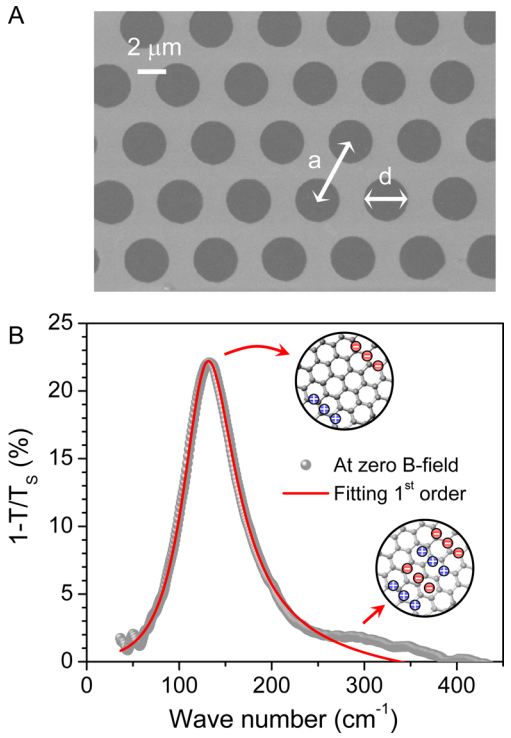

Figure 1. Scanning electron micrograph and far-infrared characterization of the graphene disk array at a zero magnetic field. (A) A scanning electron micrograph of a graphene disk array. The diameter of the disk (d) is 3 μm and the lattice constant (a) is 4.5 μm. (B) An extinction spectrum at a zero magnetic field. The solid curve is a fitting according to the plasmon resonance model using a single damped oscillator described in the Supporting Information. The deviation in the high-frequency side of the peak is due to the higher order mode. The charge distributions of the first and second order dipolar modes are illustrated in the inset.

However, in the high frequency side of the main peak in Figure 1b, there is an obvious deviation from the fit. A new mode emerges, whose origin will be discussed upon examination of the plasmon behavior in a magnetic field.

Figure 2a shows the relative transmission spectra ($T(B)/T(0)$, referenced to the zero field transmission $T(0)$) of the graphene disk array shown in Figure 1a in different magnetic fields up to 17.5 T. These spectra can also be plotted as extinction spectra ($1 - T(B)/T_s$) with reference to the bare substrate, as shown in Figure 2b. The first order dipolar plasmon resonance splits into two modes, ω^+ and ω^-. Here, the linewidths change dramatically: the upper (ω^+) branch broadens while the lower (ω^-) branch narrows with increasing B-field. At the same time, the resonance of the higher order mode shifts up in frequency, but no splitting is observed. The inset of Figure 2b shows the enlarged higher order mode portions for two spectra (at 14 and 17.5 T). The spectrum at 14 T is also fitted using a damped oscillator model (blue dashed line) and the difference between the measurement and fitting is obvious, clearly indicating the existence of the higher order mode. The oscillator strength of the higher order mode for single layer graphene is small. However, it appears more clearly for samples with two graphene layers due to stronger signals (see Supporting Information).

The Fermi level in our graphene samples is usually greater than 0.3 eV (hole doping).[24] When the magnetic field is below 20 T, the measurement conditions remain in the quasi-classical regime,[10] as is demonstrated by the linear magnetic field dependence of the cyclotron resonance frequency for the unpatterned graphene (see Supporting Information).[10,11] Assuming that carriers with mass m_c in the disk are confined by a parabolic potential, the real part of the diagonal dynamic conductivity in a magnetic field for the array is given by (see Supporting Information)

$$\mathrm{Re}\sigma_{xx}(\omega, B) = \frac{fD}{2\pi}\left[\frac{\omega^2\Gamma}{(\omega_0^2 + \omega\omega_c - \omega^2)^2 + \omega^2\Gamma^2} + \frac{\omega^2\Gamma}{(\omega_0^2 - \omega\omega_c - \omega^2)^2 + \omega^2\Gamma^2}\right] \quad (1)$$

where f is the filling factor (percentage of the graphene coverage on the sample) of the array, D is the Drude weight,[24] Γ is the scattering rate, ω_0 is the plasmon frequency at zero magnetic field, and $\omega_c = eB/m_c$ is the cyclotron resonance frequency. In the quasi-classical regime, the cyclotron mass is $m_c = |E_f|/v_f^2$, where E_f is the Fermi energy and v_f is the Fermi velocity.[10,25] In a traditional 2DEG the approximation of a parabolic confinement potential of the charge carriers in the disk usually describes the first order dipole resonance in a magnetic field very well.[13] However, the appearance of higher order modes in the spectrum is not accounted for and additional modification of the confinement potential is needed.[19,26] In a magnetic field, analysis of eq 1 reveals that the original plasmonic resonance splits into two modes with frequencies

$$\omega^{\pm} = \sqrt{\omega_0^2 + \frac{\omega_c^2}{4}} \pm \frac{\omega_c}{2} \quad (2)$$

Figure 2c shows the extracted peak frequencies obtained by fitting the spectra using two independent damped oscillators[5] (see Supporting Information) as a function of the magnetic

dx.doi.org/10.1021/nl3016335 | Nano Lett. 2012, 12, 3766−3771

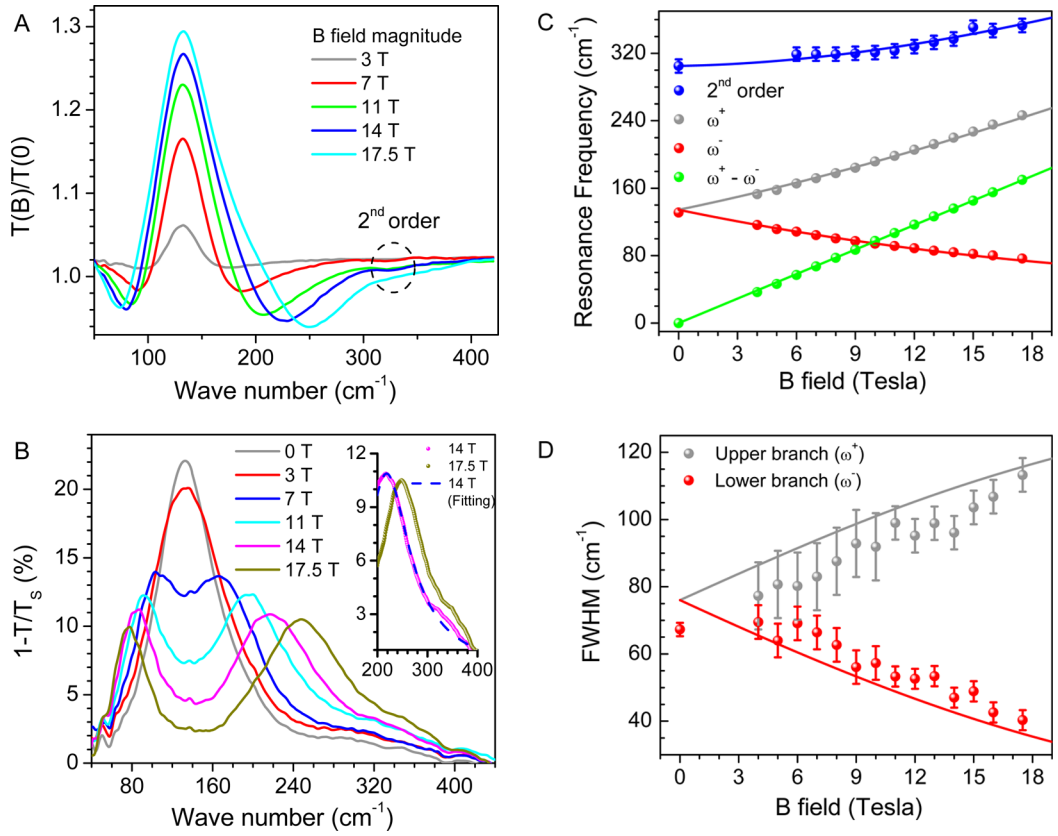

Figure 2. Magnetic field tuning of the plasmon resonance. (A) Transmission $T(B)$ through the disk array at field B, referenced to the zero field transmission. The second order dipolar mode is indicated. (B) Extinction spectra of panel A with a zero-field spectrum also shown. The inset is a zoom-in for two of the spectra to emphasize the higher order mode. The spectrum measured at 14 T is also fitted using the damped oscillator model (dashed blue line). (C) Magnetic field dependence of the peak frequencies, where the difference frequency for ω^+ and ω^- is also shown. Solid curves for first order modes are fits based on eq 2. The solid curve for the second order mode is a calculated result described in the Supporting Information. (D) Magnetic field dependence of the fwhm of the plasmon resonances. Solid curves are fits using eq 3.

field. The frequency difference between the upper and lower branches, which is the cyclotron frequency according to eq 2, is also shown, and the higher order mode frequency is plotted as well. The ω^+ and ω^- branches and their difference are fitted using eq 2 with fitting parameters ω_0 = 134 cm^{-1} and m_c = 0.096m_0, where m_0 is the free electron mass. Figure 2d shows the extracted full width at half-maximum (fwhm) $\Delta\omega$ for the ω^+ and ω^- branches. The lower branch plasmon lifetime (τ = $1/\Delta\omega$) increases from 79 to 132 fs at 17.5 T, while that for the upper branch decreases to 47 fs. These trends can be fitted using a relation for the fwhm derived directly from eq 1

$$\Delta\omega^{\pm} = \Gamma \pm \frac{2\omega_c\Gamma}{\sqrt{4\omega_0^2 + (\omega_c + \Gamma)^2} + \sqrt{4\omega_0^2 + (\omega_c - \Gamma)^2}} \quad (3)$$

where the cyclotron mass is the same as used in Figure 2c and the fitting parameter Γ = 76 cm^{-1}. Equation 3 shows that the upper branch linewidth can approach 2Γ, while that for the lower branch decreases as $1/B^2$ in the high magnetic field limit. This fitting is reasonably good and the minor deviation may be due to the doping inhomogeneity.

The plasmon lifetime tuning in the magnetic field as evidenced by the observed resonance linewidth change is remarkable, especially the sharpening of the lower frequency mode. Figure 3a shows a spectrum of a less doped graphene disk array (E_f = −0.34 eV) where the effect is even more pronounced. The bulk mode linewidth is 5 times larger than that of the edge mode. The predicted linewidth of the edge mode using eq 3 is only 20 cm^{-1}, which corresponds to a lifetime of 250 fs. The measured linewidth for the spectrum in Figure 3a is about 30 cm^{-1}, larger than the predicted value, probably due to the doping inhomogeneity. Typically, there are two factors contributing to the plasmon linewidth. One is the radiative plasmon decay[1] in which the plasmon is coupled to the electromagnetic radiation field. The radiative decay can be the dominant contribution to the plasmon resonance linewidth in noble metal particles. The other originates from the scattering of participating carriers in the collective motion by impurities and defects.[1] On the basis of the first mechanism, the plasmon lifetime can be tuned by radiative engineering of metal particle arrays.[27] In the case of the graphene plasmon in the terahertz frequency range discussed here, the radiative decay has minimal effect on the lifetime since the linewidth of the plasmon resonance corresponds very well to the Drude scattering rate obtained from the far-IR Drude response of the unpatterned graphene (see Supporting Information). As a result, the magnetic field dependence of the plasmon linewidth indicates that the field can suppress (for the ω^- branch) or enhance (for the ω^+ branch) the carrier scattering.

In order to understand this effect, we have to consider the different nature of the two modes. In a magnetic field, the plasmon in a bulk two-dimensional system has an energy gap $\hbar\omega_c$ (the cyclotron energy), which implies that the plasmon frequency should be larger than the single particle cyclotron

dx.doi.org/10.1021/nl3016335 | Nano Lett. 2012, 12, 3766−3771

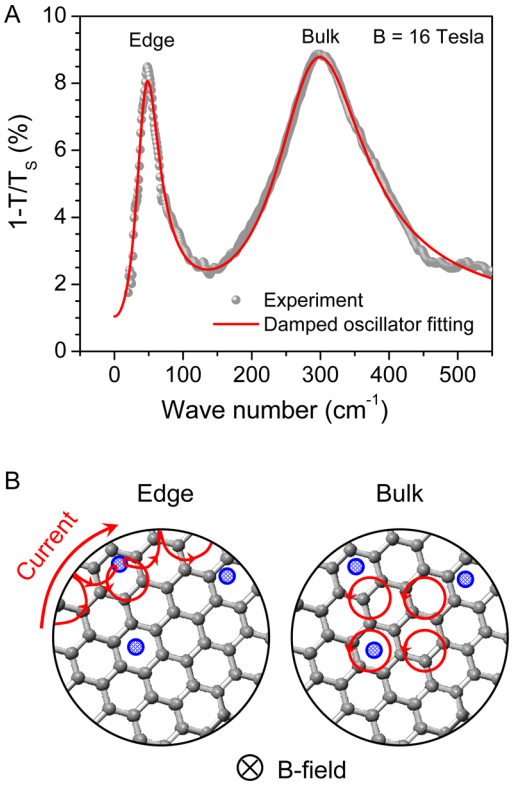

Figure 3. Edge and bulk plasmon modes. (A) An extinction spectrum for a less doped sample at 16 T. The solid curve is a fit based on two damped oscillators (Supporting Information). (B) Illustration of the charged carrier motion for the edge and bulk modes. The blue dots represent scatterers.

frequency.[13,28] The higher frequency mode (ω^+ branch) observed here has this character and corresponds to the bulk mode. As illustrated in Figure 3b, at high magnetic field the carriers participating in the bulk mode undergo cyclotron motion collectively inside the disk and are hardly affected by the confinement potential of the disk. Eventually, in the high field limit ($\omega_c \gg \omega_0$) this mode becomes the cyclotron resonance with the linewidth doubled compared to the zero field plasmon resonance (for cyclotron resonance linewidth, see Supporting Information).[10]

Appearance of the plasmon mode with lower frequency (ω^- branch) than the plasmon energy gap $\hbar\omega_c$ is attributed to the edge effect, because at the edge the Landau level bending leads to metallicity and the absence of a gap.[13,28] This mode is the so-called edge magneto-plasmon.[29] It features a current along the edge and hence a rotating dipole with frequency ω^-. The width of the edge is on the order of the cyclotron radius[13,28] which is 30 nm at 17.5 T for the sample in Figure 2. Figure 3b also illustrates the skipping orbits of the participating carriers.[16] At the edge, a scattering event by defects or impurities cannot reverse the current in a strong magnetic field, as illustrated by the orbits in Figure 3b.[16] It is the suppression of the backscattering that is responsible for the long lifetime of the edge magneto-plasmon. As in the quantum Hall effect,[16] edge effects play a crucial role in the behavior of this plasmon mode. The long lifetime of the edge plasmon can be explained from a slightly different perspective. In a high magnetic field, the rotating edge charges form the Hall current, which is almost perpendicular to the restoring electric field generated by the charges on the other side of the disk. As a result, the energy dissipation of the current is close to zero and the charges can travel for a relatively long distance along the edge. Such a suppression of the energy dissipation at the edge was widely observed in Quantum Hall Effect.

Interestingly, unlike in graphene, the linewidth for the split plasmonic peaks in traditional 2DEG disks does not seem to follow eq 3 in the terahertz frequency range:[14,15,19] the linewidths for both modes (ω^+ and ω^-) were found to be similar and to slightly decrease with increasing magnetic field. However, measurements in the radio frequency regime (megahertz to gigahertz) did show sharp edge plasmon resonances.[29] In addition, compared to traditional 2DEG, the cyclotron mass depends on the Fermi energy for Dirac Fermions in graphene,[17,18] as expected from the expression $m_c = |E_f|/v_f^2$. As a consequence, the splitting of the two plasmon branches can be tuned in graphene by doping, either electrostatically or chemically.[24] Figure 4 shows the cyclotron

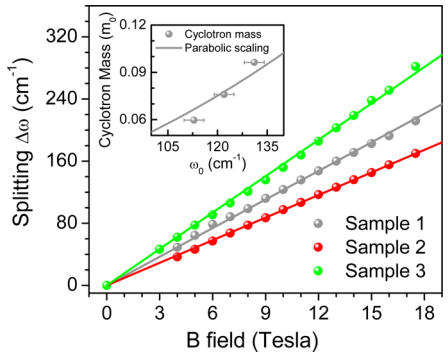

Figure 4. Doping dependence of the mode splitting. The splitting as a function of magnetic field for three samples with different doping levels. Solid lines are linear fits. The inset shows the extracted cyclotron mass for these three samples as a function of the zero field plasmon resonance frequency. The solid curve represents the parabolic scaling.

frequencies for three samples with different doping levels, determined from the splitting of the upper and lower branches in the magnetic field. The doping levels are controlled by baking or nitric acid exposure time durations. The nitric acid treatment significantly enhances the doping and at the same time leads to a moderate reduction in the scattering width.[7] The extracted cyclotron masses are plotted in the inset of Figure 4 as a function of the zero field plasmon frequencies. Since the plasmon frequency is proportional to $(E_f)^{1/2}$,[2,5] the cyclotron mass versus plasmon frequency has a parabolic scaling relation, as shown by the solid line in the inset of Figure 4.

Finally, we return to the discussion of the weak higher order mode. This mode is not described by eq 1 derived for a parabolic confinement potential. Indeed, the generalized Kohn's theorem[30,31] in the dipole approximation does not allow for the appearance of the higher order mode in the absorption spectrum for carriers confined by a parabolic potential. In our case, the typical wavelength is at least 1 order of magnitude larger than the graphene disk diameter, and the dipole approximation is satisfied. Appearance of the higher order mode is therefore an indication of the breakdown of Kohn's theorem.[26] In slightly doped graphene under a strong magnetic field, this theorem is inherently inapplicable because of the linear band structure of graphene.[20,32] However, at higher doping levels, the Landau levels near the Fermi surface

dx.doi.org/10.1021/nl3016335 | Nano Lett. 2012, 12, 3766−3771

are not well separated, and Kohn's theorem is asymptotically valid.[33] Therefore, we attribute the breakdown of Kohn's theorem to the anharmonicity of the confinement potential. We are not able to obtain the detailed form of the confinement potential from the measured extinction spectra. The confinement potential depends on the fixed charge distribution, especially in the regions close to the edge, which can be affected by the lithographical patterning process. Nevertheless, it seems that an anharmonic potential within the graphene disk is closer to the reality than an idealized harmonic potential. In previous studies of traditional 2DEG quantum dot with the shape of the dots deviating from the circular shape, higher order edge modes were observed,[13,15,26] obviously due to the anharmonic confinement introduced by the dot geometry. However, the higher order mode observed in our graphene disks does not evolve into an edge mode in a magnetic field, which is different from the first order mode as well as other higher order modes observed previously in the traditional 2DEG quantum dots.[15,26] This mode is a second order dipolar mode, which was previously predicted by theory.[19] The inset of Figure 1B depicts the charge distribution for this mode and the first order dipolar mode. To the best of our knowledge, this is the first time that this mode has been observed experimentally. Calculation of the frequency of this mode in a magnetic field according to theoretical predictions[19] (see Supporting Information) results in excellent agreement with the experimental observations (Figure 2c).

In summary, we show that the plasmon lifetime in graphene can be continuously tuned using a magnetic field and that the mode splitting can be tuned through doping. In addition, the observation of a higher order dipolar mode indicates the anharmonicity of the confinement potential in graphene disks. The results demonstrate that graphene is a very promising material for plasmonics and magneto-optics studies, and that magneto-plasmon spectroscopy opens a new avenue to study graphene edge effects. Other intriguing phenomena may be found in the quantum regime, where the carriers are distributed in only a few Landau levels.

After finishing this manuscript, we became aware of a paper[34] by Crassee et al. that reports the observation of magneto-plasmons from as-grown epitaxial graphene on silicon carbide due to the substrate terraces and wrinkles.

■ ASSOCIATED CONTENT

Supporting Information

Details of the relation between the extinction spectrum and dynamic conductivity, cyclotron resonance of the unpatterned graphene, plasmon line width, derivation of eq 1, calculation procedures of the second order dipolar mode frequencies, and the additional data for the two-layer disk array. This material is available free of charge via the Internet at http://pubs.acs.org.

■ AUTHOR INFORMATION

Corresponding Author

*E-mail: hyan@us.ibm.com (H.Y.); avouris@us.ibm.com (P.A.); fxia@us.ibm.com (F.X.).

Author Contributions

§These authors contributed equally.

Notes

The authors declare no competing financial interest.

■ ACKNOWLEDGMENTS

The authors are grateful to B. Ek and J. Bucchignano for technical supports, to T. Low and V. Perebeinos for helpful discussions, and to D. Farmer for proof reading of this manuscript. Part of this work was performed at the National High Magnetic Field Laboratory, which is supported by NSF/DMR-0654118, the State of Florida, and DOE.

■ REFERENCES

(1) Maier, S. *Plasmonics: Fundamentals and Applications*, 1st ed.; Springer: New York, 2007.
(2) Koppens, F. H. L.; Chang, D. E.; Javier Garcia de Abajo, F. *Nano Lett.* **2011**, *11*, 3370−3377.
(3) Vakil, A.; Engheta, N. *Science* **2011**, *332*, 1291−1294.
(4) Thongrattanasiri, S.; Koppens, F. H. L.; Garcia de Abajo, F. J. *Phys. Rev. Lett.* **2012**, *108*, 047401.
(5) Ju, L.; Geng, B.; Horng, J.; Girit, C.; Martin, M.; Hao, Z.; Bechtel, H. A.; Liang, X.; Zettl, A.; Shen, Y. R.; Wang, F. *Nat. Nanotechnol.* **2011**, *6*, 630−634.
(6) Fei, Z.; Andreev, G. O.; Bao, W.; Zhang, L. M.; S. McLeod, A.; Wang, C.; Stewart, M. K.; Zhao, Z.; Dominguez, G.; Thiemens, M.; Fogler, M. M.; Tauber, M. J.; Castro-Neto, A. H.; Lau, C. N.; Keilmann, F.; Basov, D. N. *Nano Lett.* **2011**, *11*, 4701−4705.
(7) Yan, H.; Li, X.; Chandra, B.; Tulevski, G.; Wu, Y.; Freitag, M.; Zhu, W.; Avouris, P.; Xia, F. *Nat. Nanotechnol.* **2012**, *7*, 330.
(8) Abedinpour, S. H.; Vignale, G.; Principi, A.; Polini, M.; Tse, W.-K.; MacDonald, A. H. *Phys. Rev. B* **2011**, *84*, 045429.
(9) Bostwick, A.; Speck, F.; Seyller, T.; Horn, K.; Polini, M.; Asgari, R.; MacDonald, A. H.; Rotenberg, E. *Science* **2010**, *328*, 999−1002.
(10) Witowski, A. M.; Orlita, M.; Stepniewski, R.; Wysmolek, A.; Baranowski, J. M.; Strupinski, W.; Faugeras, C.; Martinez, G.; Potemski, M. *Phys. Rev. B* **2010**, *82*, 165305.
(11) Crassee, I.; Levallois, J.; Walter, A. L.; Ostler, M.; Bostwick, A.; Rotenberg, E.; Seyller, T.; van der Marel, D.; Kuzmenko, A. B. *Nat. Phys.* **2010**, *7*, 48−51.
(12) Kono, J., Cyclotron resonance. In *Methods in Materials Research*; Kaufmann, E. N., Ed.; Wiley: New York, 2001.
(13) Kushwaha, M. S. *Surf. Sci. Rep.* **2001**, *41*, 1−416.
(14) Allen, S. J.; Stormer, H. L.; Hwang, J. C. M. *Phys. Rev. B* **1983**, *28*, 4875−4877.
(15) Demel, T.; Heitmann, D.; Grambow, P.; Ploog, K. *Phys. Rev. Lett.* **1990**, *64*, 788.
(16) Buttiker, M. *Phys. Rev. B* **1988**, *38*, 9375−9389.
(17) Novoselov, K. S.; Geim, A. K.; Morozov, S. V.; Jiang, D.; Katsnelson, M. I.; Grigorieva, I. V.; Dubonos, S. V.; Firsov, A. A. *Nature* **2005**, *438*, 197−200.
(18) Zhang, Y.; Tan, Y.; Stormer, H. L.; Kim, P. *Nature* **2005**, *438*, 201−204.
(19) Ye, Z. L.; Zaremba, E. *Phys. Rev. B* **1994**, *50*, 17217.
(20) Roldan, R.; Fuchs, J. N.; Goerbig, M. O. *Phys. Rev. B* **2010**, *82*, 205418.
(21) Bychkov, Y. A.; Martinez, G. *Phys. Rev. B* **2008**, *77*, 125417.
(22) Wang, W.; Apell, P.; Kinaret, J. *Phys. Rev. B* **2011**, *84*, 085423.
(23) Li, X.; Cai, W.; An, J.; Kim, S.; Nah, J.; Yang, D.; Piner, R.; Velamakanni, A.; Jung, I.; Tutuc, E.; Banerjee, S. K.; Colombo, L.; Ruoff, R. S. *Science* **2009**, *324*, 1312−1314.
(24) Yan, H.; Xia, F.; Zhu, W.; Freitag, M.; Dimitrakopoulos, C.; Bol, A. A.; Tulevski, G.; Avouris, P. *ACS Nano* **2011**, *5*, 9854−9860.
(25) Zheng, Y.; Ando, T. *Phys. Rev. B* **2002**, *65*, 245420.
(26) Heitmann, D.; Bollweg, K.; Gudmundsson, V.; Kurth, T.; Riege, S. P. *Physica E* **1997**, *1*, 204−210.
(27) Adato, R.; Yanik, A. A.; Wu, C.-H.; Shvets, G.; Altug, H. *Opt. Express* **2010**, *18*, 4526−4537.
(28) Volkov, V. A.; Mikhailov, S. A. *JETP Lett.* **1988**, *67*, 1639−1653.
(29) Mast, D. B.; Dahm, A. J.; Fetter, A. L. *Phys. Rev. Lett.* **1985**, *54*, 1706−1709.
(30) Kohn, W. *Phys. Rev.* **1961**, *123*, 1242−1244.

(31) Maksym, P. A.; Chakraborty, T. *Phys. Rev. Lett.* **1990**, *65*, 108−111.
(32) Henriksen, E. A.; Cadden-Zimansky, P.; Jiang, Z.; Li, Z. Q.; Tung, L. C.; Schwartz, M. E.; Takita, M.; Wang, Y. J.; Kim, P.; Stormer, H. L. *Phys. Rev. Lett.* **2010**, *104*, 067404.
(33) Muller, M.; Fritz, L.; Sachdev, S. *Phys. Rev. B* **2008**, *78*, 115406.
(34) Crassee, I.; Orlita, M.; Potemski, M.; Walter, A. L.; Ostler, M.; Seyller, T.; Gaponenko, I.; Chen, J.; Kuzmenko, A. B. *Nano Lett.* **2012**, *12*, 2470.

dx.doi.org/10.1021/nl3016335 | *Nano Lett.* 2012, 12, 3766−3771